Progress In Electromagnetics Research, Vol. 135, 137–149, 2013

A TIME-DOMAIN APPROACH FOR THE FAST DESIGN OF REFLECTOR IMPULSE-RADIATING ANTENNAS

Linglu Chen*, Ju Feng, Lei Chang, and Cheng Liao

Institute of Electromagnetics, Southwest Jiaotong University, Chengdu, Sichuan 610031, China

Abstract—It is difficult to determine the feed radiation center and F/D of the reflector impulse-radiating antenna (IRA) in frequency-domain, due to its ultra-wideband (UWB) property. This paper presents an efficient approach to design the reflector IRAs, via evaluating the transient radiation patterns (TRPs) of the feed for some given different radiation centers. Only one time-domain simulation for the feed is needed in this method. Comparing with the global optimization algorithms, our method is fast and reliable in the design of the reflector IRAs.

1. INTRODUCTION

The impulse-radiating antennas (IRAs) have many applications in electromagnetic compatibility/electromagnetic interference (EMC/EMI) [1–3], ultra-wideband (UWB) communications [4–11], target detection and identification [12–14], medical therapies and imaging [15–18], etc. The paraboloidal reflector has been commonly used as an optical focusing device in the IRAs [1]. Two important conditions should be satisfied in order to obtain the largest bore-sight gain of the reflector IRAs. One is to set the feed radiation center coincident with the optical focal point of the paraboloid. The other is to select a suitable F/D of the reflector basing on the required reflector edge taper [19, 20]. However, it is almost impossible to find the ideal radiation center of the UWB feed in frequency-domain. On the other hand, an accessible radiation pattern, which can synchronously evaluate the amplitude and time-delay of the radiated pulses in time-domain, is not known [6]. Although various numerical methods, such as the finite difference time

Received 14 November 2012, Accepted 12 December 2012, Scheduled 13 December 2012

* Corresponding author: Linglu Chen (zjwycll@163.com).

domain (FDTD) method, have been applied in the design of reflector IRAs, they need to be done for many times and a lot of computing time are required [21–23].

In this paper, a fast approach for the design of the reflector IRAs is proposed. The feed's transient radiation pattern (TRP) is defined as the spherical electric field distribution at the peak of the feed bore-sight radiated pulse. For different radiation centers, the TRPs can be calculated by the compensation of space and time according to the data, which can be obtained via only one time-domain simulation of the feed. For each TRP, the subtended angle of the reflector, which is related to F/D, can be determined with a given reflector edge taper. Finally, an evaluation function is introduced in selecting a proper TRP, which has a gentle attenuation within the subtended angle and decays rapidly outside the angle. The parameters we need to determine are the radiation center and F/D corresponding to the selected TRP. Numerical examples show that our method can quickly obtain the optimal reflector IRA which has the largest bore-sight gain.

The remainder of this paper is organized as follows. Section 2 introduces our method in detail. In Section 3 we discuss the reflector edge taper for the best performance of the reflector IRAs on the bore-sight, and demonstrate the advantages of our method over several global optimization algorithms. Conclusions are given in Section 4.

2. THE TIME-DOMAIN APPROACH FOR REFLECTOR IRAS DESIGN

The property of IRAs is to generate a fast-rising field on the aperture and produce an impulse-like far field [24]. Here we focus on the electric field distribution at the peak of the bore-sight radiated pulse of the feed, which is related to the moment that the fast-rising field is generated on the reflector aperture.

2.1. The Computation of TRPs

This method for the calculation of TRPs is based on the condition that the UWB feed radiates pulses in certain spatial directions with different time-delay and amplitude attenuation, but without serious distortion.

The approximate radiation center of an axis-symmetric feed will be on the bore-sight and near the feed aperture [25]. As shown in Fig. 1, the bore-sight of the feed is along the z-axis, the feed aperture center is at the origin O, point C represents the feed's radiation center, L denotes the length of the feed, and usually $|CO| < L$.

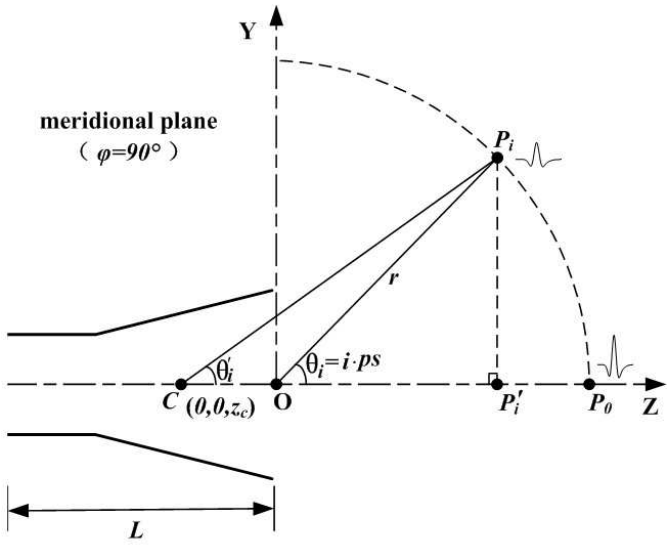

Figure 1. Schematic of the method for the calculation of TRPs.

Sampling points P_i are selected along the circle for the radius of r, with the same angular interval ps in the range of $0° \leq \theta \leq 90°$, both on the azimuth plane ($\varphi = 0°$) and the meridional plane ($\varphi = 90°$).

Now a time-domain simulation for the feed is performed. The time-domain response at P_i is recorded as $E_i(t)$, where i is the integer from 0 to N, and $N = \lfloor 90/ps \rfloor$. The time for the peak of $E_i(t)$ is denoted as tp_i.

We compute the TRP at different positions C_m along z-axis in $[z_{\text{cmin}}, z_{\text{cmax}}]$ with the space step $\triangle z$, where m is the integer from 1 to M, and $M = \lfloor (z_{\text{cmax}} - z_{\text{cmin}})/\triangle z + 1 \rfloor$. Since $r \gg L$, the sampling points in the angle of θ are almost uniform.

The normalized TRP at the point C_m can be written as:

$$E_{cm}(\varphi, \theta'_{mi}) = AF(\varphi, \theta'_{mi}) + 20 \lg \left(\frac{E_0(tp_0 - \triangle t\,(\varphi, \theta'_{mi}))}{E_0(tp_0)} \right), \qquad (1)$$

where $\varphi = 0°$ or $90°$ represents different observation planes, as well as $\theta'_{mi} = \arccos(|C_m P'_i|/|C_m P_i|)$ is the radiation angle, the point P'_i is the projection of P_i on the z-axis, $|C_m P'_i| = r\cos(\theta_i) - z_{cm}$, $|C_m P_i| = \sqrt{|C_m P'_i|^2 + |P_i P'_i|^2}$, and $|P_i P'_i| = r\sin(\theta_i)$.

$AF(\varphi, \theta'_{mi})$ is the amplitude attenuation factor:

$$AF\left(\varphi, \theta'_{mi}\right) = 20 \lg \left(\frac{|C_m P_i| E_i(tp_i)}{|C_m P_0| E_0(tp_0)} \right) + SA\left(\varphi, \theta'_{mi}\right), \qquad (2)$$

where $SA(\varphi, \theta'_{mi}) = 20\lg\left(\left(1+\cos\left(\theta'_{mi}\right)\right)/2\right)$ is the space attenuation factor [26].

$\triangle t(\varphi, \theta'_{mi})$ is the time delay factor:

$$\triangle t\left(\varphi, \theta'_{mi}\right) = tp_i - \left(|C_m P_i| - |C_m P_0|\right)/c - tp_0, \tag{3}$$

where c presents the light speed.

2.2. The Selection of Radiation Center

For a given reflector edge taper ET, the subtended angle θ'_{ms} of the reflector can be easily obtained via the corresponding TRP at C_m. Here, $\theta'_{ms} = \min(\theta'_{ms0}, \theta'_{ms90})$. θ'_{ms0} and θ'_{ms90} are the subtended angle of the reflector in the azimuth plane and meridional plane, respectively.

The more consistent the feed radiation patterns in the azimuth plane and meridional plane are, the better far-field response of the reflector IRA is [27]. Therefore, a series of radiation centers, which meet the condition $|E_{cm}(0, \theta'_{ms}) - E_{cm}(90, \theta'_{ms})| \leq IT$, are selected first and denoted as the set **CS**. IT is the inconsistency tolerance, and usually $1 \leq IT \leq 2$.

Then, an evaluation function is introduced in determining the most suitable radiation center in the set of **CS**. The evaluation function can be written as:

$$f(C_m) = w1 \cdot AG(C_m) + w2 \cdot AR(C_m), \tag{4}$$

where the $w1$ and $w2$ are the weights. In this paper, they are chosen as 0.9 and 0.1, respectively.

$$AG(C_m) = -\sum_{i=0}^{s} \sum_{\varphi=0,90} \frac{E_{cm}(\varphi, \theta'_{mi})}{2(s+1)}, \tag{5}$$

here, the minimization of AG requires that the transient electric field within $0 \leq \theta'_{mi} \leq \theta'_{ms}$ should attenuate as gentle as possible.

$$AR(C_m) = \sum_{i=s+1}^{N} \sum_{\varphi=0,90} \frac{E_{cm}\left(\varphi, \theta'_{mi}\right)}{2(N-s)}, \tag{6}$$

here, the minimization of AR requires that the transient electric field within $\theta'_{m(s+1)} \leq \theta'_{mi} \leq \theta'_{mN}$ should attenuate as fast as possible.

The C_m corresponding to the $\min(\mathbf{f})$ is the most suitable radiation center, and the F/D can be obtained by:

$$k_m = \frac{1+\sqrt{1+\tan(\theta'_{ms})^2}}{4\tan(\theta'_{ms})}. \tag{7}$$

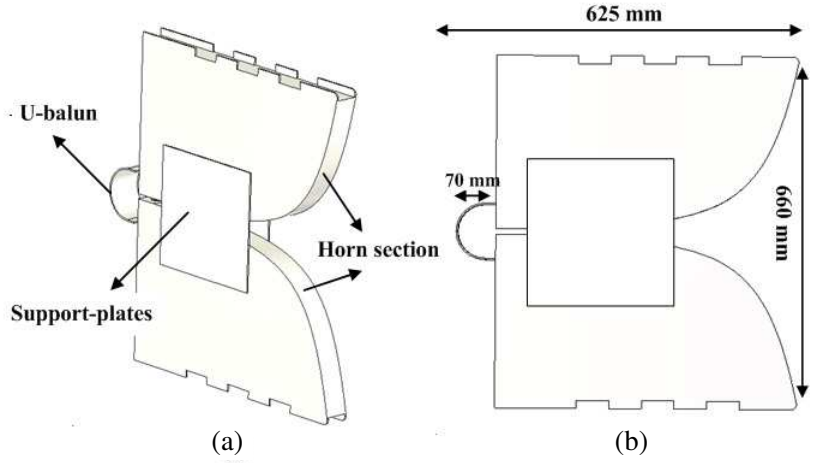

Figure 2. Structure of the knife-shape TEM horn.

3. NUMERICAL RESULTS

The TEM horn has been commonly used to feed the reflector IRAs [28, 29]. In this section, a knife-shape TEM horn [30], which exhibits good performance from 120 MHz to 1250 MHz, is applied to feed a paraboloidal reflector. The aperture diameter of the reflector is 3 m. The length, width, and height of this feed are 62.5 cm, 5 cm, and 66 cm, respectively. Its structure is shown in Fig. 2. The Gaussian pulse and Differential Gaussian pulse with the width of 1.6 ns and 2 ns, respectively, are employed to excite the feed. The peak power is 1 W in both pulses.

3.1. The Discussion of *ET*

The feed is simulated by the electromagnetic solver CST MWS, with the angular interval $ps = 2^\circ$ and the reference radius $r = 100$ m. The radiation center moves from $z_{\min} = -500$ mm to $z_{\max} = 500$ mm with $\triangle z = 5$ mm. The TRPs are calculated via Equation (1).

The radiated pulses with different excitations are shown in Figs. 3 and 4.

When the feed is excited by a Gaussian pulse, the radiated pulses of the feed in the far field exhibit double peaks (see Fig. 3(a)). The TRPs are calculated for the negative (first) and positive (second) peak moments tp_i respectively. The results with different ET are given in Table 1. The $|R \cdot E_p|$ is used to measure the radiation ability of the

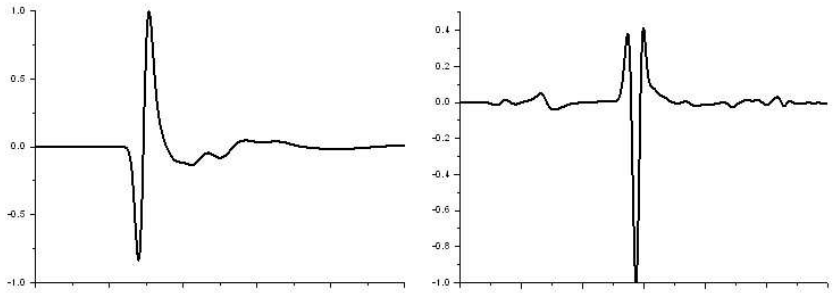

Figure 3. The radiated pulses excited by Gaussian pulse: (a) feed and (b) reflector IRA.

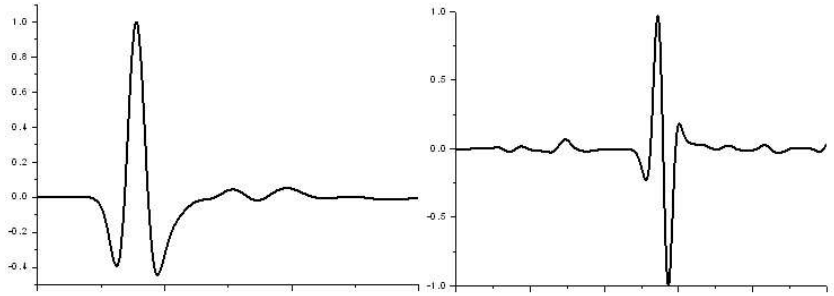

Figure 4. The radiated pulses excited by differential Gaussian pulse: (a) feed and (b) reflector IRA.

reflector IRA, where R is the radiation distance ($R = 100\,\mathrm{m}$ is chosen in this paper), E_p presents the single peak value of the radiated pulse on the bore-sight of the reflector IRA in this example (see Fig. 3(b)).

As shown in Table 1, the values of $|R \cdot E_p|$ for the the first peak are larger than the ones for the second peak. Hence, recording the tp_i with the first peak is more effective in our method, when the feed's radiation pulses have multiple peaks. It can also be seen from Table 1 that the radiation centers for the range of $-15\,\mathrm{dB} \leq ET \leq -10\,\mathrm{dB}$ are close.

Table 2 presents the case for the excitation of the Differential Gaussian pulse. Since the radiated pulses of the reflector IRA have double peaks in the far field (see Fig. 4(b)), the E_p is the peak-to-peak value of the radiated pulse.

Table 1. Results with different ET. The feed is excited by Gaussian pulse.

ET (dB)	First Peak			Second Peak		
	Radiation Center (mm)	F/D	$\|R \cdot E_p\|$ (V)	Radiation Center (mm)	F/D	$\|R \cdot E_p\|$ (V)
-9	-285	0.52	48.60	-380	0.66	45.90
-10	-235	0.47	48.77	-255	0.51	48.74
-11	-235	0.47	48.77	-255	0.47	48.41
-15	-200	0.37	46.28	-290	0.40	45.04
-17	-160	0.32	44.49	-300	0.39	43.94
-20	-130	0.27	42.20	-315	0.37	41.52

Table 2. Results with different ET. The feed is excited by differential Gaussian pulse.

ET (dB)	Radiation Center (mm)	F/D	$\|R \cdot E_p\|$ (V)
-9	0	0.59	115.87
-10	-205	0.42	129.93
-11	-195	0.39	127.27
-15	-210	0.32	114.93
-17	-210	0.31	111.79
-20	-230	0.30	105.30

It can be seen from Table 2 that the radiation centers for the range of $-20\,\text{dB} \leq ET \leq -10\,\text{dB}$ are close. Thus, the TRPs of them are relatively stable, and the $|R \cdot E_p|$ is more sensitive to the F/D. Fig. 5 gives the TRPs corresponding to $ET = -10\,\text{dB}$, $-15\,\text{dB}$ and $-20\,\text{dB}$, when the feed is excited by the Differential Gaussian pulse. The corresponding normalized energy patterns of the reflector IRA in the meridional plane are shown in Fig. 6.

It can be seen from Fig. 6 that the energy is more concentrated on the bore-sight when $ET = -10\,\text{dB}$, but the front to back ratio is worse in this case. The side-lobe level of them are almost unchanged. These performances are similar to the conclusion of the frequency-domain reflector antennas design, i.e., $-10\,\text{dB}$ is recommended for the reflector edge taper to obtain the largest gain on the bore-sight. Furthermore, it can be seen from Tables 1 and 2 that the value of $|R \cdot E_p|$ corresponding

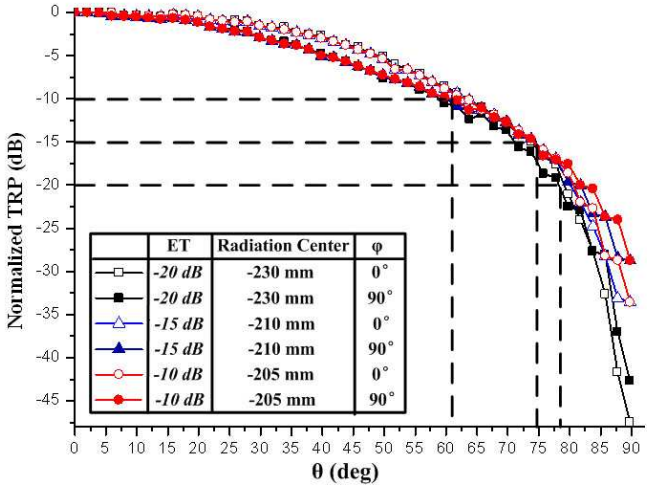

Figure 5. The TRPs corresponding to $ET = -10\,\text{dB}$, $-15\,\text{dB}$ and $-20\,\text{dB}$. The feed is excited by differential Gaussian pulse.

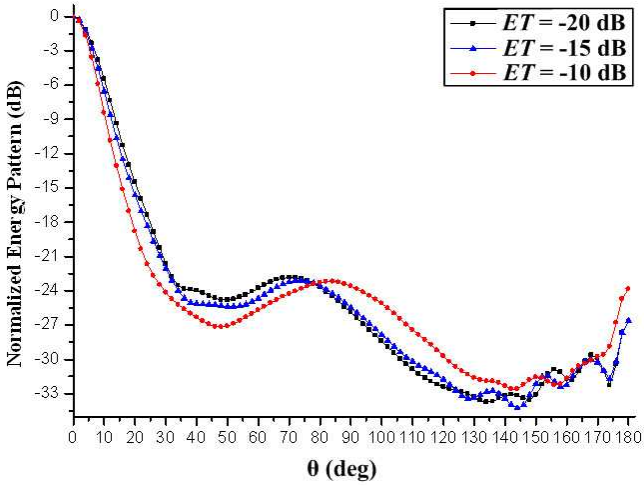

Figure 6. The normalized energy patterns of the reflector IRA in the meridional plane. The feed is excited by differential Gaussian pulse.

Table 3. Optimal results of the reflector IRA obtained by different algorithms.

	Gaussian Pulse			Differential Gaussian Pulse		
	Radiation Center (mm)	F/D	$\lvert R \cdot E_p \rvert$ (V)	Radiation Center (mm)	F/D (V)	$\lvert R \cdot E_p \rvert$
This paper	−235	0.47	48.77	−205	0.42	129.93
DES	−223.36	0.4684	48.80	−205.14	0.4270	130.48
Taguchi	−226.75	0.4658	48.79	−205.60	0.4275	130.48
HSM-based EGO	−223.41	0.4673	48.80	−205.60	0.4252	130.48

to $ET = -10\,\text{dB}$ is the largest. Therefore, the $ET = -10\,\text{dB}$ is chosen in our method.

3.2. The Comparisons with Several Global Optimization Algorithms

In order to show the performance of our approach, we also apply the differential evolution strategy (DES) [31], Taguchi's method [32] and hybrid-surrogate-model-based EGO algorithm (HSM-based EGO) [33] to optimize the $|R \cdot E_p|$ of the reflector IRA respectively. The design parameters are the radiation center and F/D, with the ranges of $[-500\,\text{mm},\ 500\,\text{mm}]$ and $[0.2,\ 1]$ respectively. The best solutions obtained by these three algorithms in 10 independent runs are listed in Table 3.

It can be seen from Table 3 that the results obtained by our method are almost the same as those optimized by the three global optimization algorithms. The little difference between our results and those from the global optimization algorithms might come from the discrete data used in our method, and this difference can be ignored in engineering applications. These comparisons demonstrate that our method is very effective in the design of reflector IRAs.

4. CONCLUSIONS

An universal approach for the fast design of reflector IRAs is proposed in this paper. We only focus on the electric field distribution at the peak moment for the feed's bore-sight radiated pulse, which is important to the generation of a fast-rising field on the reflector aperture. Only one time-domain simulation of the feed is required

for the calculation of TRPs with different radiation centers in this approach. An evaluation function is applied to evaluate the TRPs for a given ET. Numerical examples show that $ET = -10\,\mathrm{dB}$ is a good choice for obtaining the largest gain on the bore-sight of the reflector IRAs. The comparisons with several global optimization algorithms show that our method is reliable and efficient in the design of reflector IRAs.

ACKNOWLEDGMENT

This work was supported by the National Basic Research Program of China (973 Program, Grant No. 2013CB328904), the NSAF of China (Grant No. 11076022), and the Research Fund of Key Laboratory of HPM Technology (Grant No. 2012-LHWJJ.006).

REFERENCES

1. Tyo, J. S., E. G. Farr, and D. I. Lawry, "Effect of defocus on the prompt response of a reflector IRA," *IEEE Transactions on Antennas and Propagation*, Vol. 53, 3247–3254, 2005.
2. Chung, J.-Y., "Ultra-wideband dielectric-loaded horn antenna with dual-linear polarization capability," *Progress In Electromagnetics Research*, Vol. 102, 397–411, 2010.
3. Radasky, W. A., C. E. Baum, and M. W. Wik, "Introduction to the special issue on high-power electromagnetics (HPEM) and intentional electromagnetic interference (IEMI)," *IEEE Transactions on Electromagnetic Compatibility*, Vol. 46, 314–321, 2004.
4. Ban, Y.-L., H.-M. Yuan, J.-H. Chen, J. L.-W. Li, and Y.-J. Wu, "A novel ultra-wideband antenna with distributed inductance for wireless USB dongle attached to laptop computer," *Journal of Electromagnetic Waves and Applications*, Vol. 26, Nos. 2–3, 179–191, 2012.
5. Chang, L., C. Liao, L.-L. Chen, W. Lin, X. Zheng, and Y.-L. Wu, "Design of an ultra-wideband power divider via the coarse-grained parallel micro-genetic algorithm," *Progress In Electromagnetics Research*, Vol. 124, 425–440, 2012.
6. Pancera, E., T. Zwick, and W. Wiesbeck, "Spherical fidelity patterns of UWB antennas," *IEEE Transactions on Antennas and Propagation*, Vol. 59, 2111–2119, 2011.
7. Jo, N.-I., C.-Y. Kim, D.-O. Kim, and H.-A. Jang, "Compact ultra-wideband antenna with quadruple-band rejection characteristics

using SRR/CSRR structure," *Journal of Electromagnetic Waves and Applications*, Vol. 26, Nos. 5–6, 583–592, 2012.

8. Zhu, X., H. L. Xiong, Q. Yu, and K. C. Yi, "Single link tracking scheme based on UWB localization.," *Journal of Systems Engineering and Electronics*, Vol. 20, No. 6, 1207–1212, 2009.
9. Li, W.-T. and Y.-Q. Hei, "Design of ultrawideband antenna with multiple band-notched characteristics," *Journal of Electromagnetic Waves and Applications*, Vol. 26, No. 7, 942–951, 2012.
10. Chen, Z. and Y.-P. Zhang, "Effects of antennas and propagation channels on synchronization performance of a pulse-based ultrawideband radio system," *Progress In Electromagnetics Research*, Vol. 115, 95–112, 2011.
11. Li, B., Z. Zhou, D. Li, and S. Zhai, "Efficient cluster identification for measured ultra-wideband channel impulse response in vehicle cabin," *Progress In Electromagnetics Research*, Vol. 117, 121–147, 2011.
12. Bajracharya, C., X. Shu, C. E. Baum, and K. H. Schoenbach, "Target detection with impulse radiating antenna," *IEEE Antennas and Wireless Propagation Letters*, Vol. 10, 496–499, 2011.
13. Harmer, S. W., S. E. Cole, N. J. Bowring, N. D. Rezgui, and D. Andrews, "On body concealed weapon detection using a phased antenna array," *Progress In Electromagnetics Research*, Vol. 124, 187–210, 2012.
14. Mao, S. G., J. C. Yeh, and S. L. Chen, "Ultrawideband circularly polarized spiral antenna using integrated balun with application to time-domain target detection," *IEEE Transactions on Antennas and Propagation*, Vol. 57, No. 7, 1914–1920, 2009.
15. Kumar, P., C. E. Baum, S. Altunc, J. Buchenauer, X. Shu, C. G. Christodoulou, E. Schamiloglu, and K. H. Schoenbach, "A hyperband antenna to launch and focus fast high-voltage pulses onto biological targets," *IEEE Transactions on Microwave Theory and Techniques*, Vol. 59, No. 4, 1090–1101, 2011.
16. O'Halloran, M., M. Glavin, and E. Jones, "Rotating antenna microwave imaging system for breast cancer detection," *Progress In Electromagnetics Research*, Vol. 107, 203–217, 2010.
17. Chen, Y. F., I. J. Craddock, P. Kosmas, M. Ghavami, and P. Rapajic, "Multiple-input multiple-output radar for lesion classification in ultrawideband breast imaging," *IEEE Journal of Selected Topics in Signal Processing*, Vol. 4, No. 1, 187–201, 2010.
18. Zanoon, T. F. and M. Z. Abdullah, "Early stage breast cancer

detection by means of time-domain ultra-wide band sensing," *Measurement Science and Technology*, Vol. 22, No. 11, 114016, 2011.

19. Park, J. H., H. K. Choi, and S. H. Kim, "Design of Ku-band reflectarray using hexagonal patch with crossed slots," *Microwave and Optical Technology Letters*, Vol. 54, No. 10, 2383–2387, 2012.
20. Schejbal, V., J. Pidanic, and O. Fiser, "Broadband approximation of radiation patterns for doubly curved reflector antennas," *IEEE Antennas and Propagation Magazine*, Vol. 53, No. 6, 140–146, 2011.
21. Guo, C., A. X. Zhang, H. Wu, Y. S. Jiang, and W. B. Wang, "A high-power reflector impulse antenna with dual-tem source," *International Journal of Infrared and Millimeter Waves*, Vol. 29, No. 9, 832–838, 2008.
22. Lee, K. H., C. C. Chen, and R. Lee, "UWB dual-linear polarization dielectric horn antennas as reflector feeds," *IEEE Transactions on Antennas and Propagation*, Vol. 55, No. 3, 798–804, 2007.
23. Lisitsyn, V. P, "A parabolic antenna for the radiation power UWB pulses on the basis of the satellite dish," *2006 IEEE Antennas and Propagation Society International Symposium*, 811, 2006.
24. Baum, C. E., "Radiation of impulse-like transient fields," *Sensor and Simulation Notes*, Note 321, 1989.
25. Yi, C. L., S. T. Zhu, Y. J. Fan, and W. F. Xia, "Time-domain method of determining radiation centers of ultra wideband antennas," *High Power Laser and Particle Beams*, Vol. 23, No. 5, 1312–1314, 2011.
26. Zhang, X. G., G. Wu, and Y. Zhong, "The phase optimization of the paraboloidal reflectarray antenna on satellite," *Chinese Journal of Radio Science*, Vol. 27, No. 1, 197–202, 2012.
27. Plastikov, A. N. and N. M. Feizulla, "Simulation of array fed scanning reflector antenna with small beam shift step," *Journal of Radio Electronics*, Vol. 6, 15–15, 2012.
28. Liao, Y., P. Xie, and W. Lu, "Cassegrain dual reflector antenna for UWB high power microwave," *High Power Laser and Particle Beams*, Vol. 19, No. 8, 1329–1332, 2007.
29. Yi, C. L., S. T. Zhu, and Y. J. Fan, "Ultrawide band dual-pulse radiating antenna," *High Power Laser and Particle Beams*, Vol. 22, No. 5, 1081–1084, 2010.
30. Chen, L. L., C. Liao, L. Chang, X. Zheng, G. Su, and J. Fang, "A novel ultra-wideband knife-shape TEM horn antenna design

for transient application," *2010 International Conference on Microwave and Millimeter Wave Technology Proceedings*, 355–358, 2010.

31. Dib, N. I., S. K. Goudos, and H. Muhsen, "Application of Taguchi's optimization method and self-adaptive differential evolution to the synthesis of linear antenna arrays," *Progress In Electromagnetics Research*, Vol. 102, 159–180, 2010.
32. Li, R., L. Xu, X.-W. Shi, N. Zhang, and Z.-Q. Lv, "Improved differential evolution strategy for antenna array pattern synthesis problems," *Progress In Electromagnetics Research*, Vol. 113, 429–441, 2011.
33. Chen, L.-L., C. Liao, W. Lin, L. Chang, and X.-M. Zhong, "Hybrid-surrogate-model-based efficient global optimization for high-dimensional antenna design," *Progress In Electromagnetics Research*, Vol. 124, 85–100, 2012.